THEORETICAL CRITICAL FIELD IN RF APPLICATION

K.Saito #, KEK, Accelerator Lab, 1-1, Oho, Tsukuba-shi,
Ibaraki-ken, Japan

Abstract

For these ten years, the high gradient of niobium superconducting RF (SRF) cavities seems to be saturated around 40 MV/m. The question is in the further technical R&D or in the fundamental critical field of niobium material. In this paper the author will try to explain the saturation from the theoretical point of view. By Abrikosov theory based on Ginzburg Landau equation, superheating field is reviewed as the fundamental critical field in RF application. Abriksov theory is available only for the temperatures close to the critical temperature (T_C) or the small band gaps. Supposing the small band gap in such a high gradient 40MV/m, the concept of superheating field is expanded the low temperatures around 2K. In this paper, from the temperature variations of λ, ξ and H_C the temperature dependent superheating field is deduced. The results will be compared with experimental RF critical fields of Nb, Nb_3Sn and Pb superconducting RF cavities. One will see good agreements between the theory and the experimental results. The result in this work strongly suggests the vortex line nucleation is more likely the mechanism of theoretical critical field in RF application.

INTRODUCTION

The Situation of The Current High Gradient in SRF Niobium Cavities

As shown Fig.1, to date bulk niobium superconducting RF (SRF) cavities have achieved 40 MV/m with the accelerating gradient: Eacc at 1.5 - 2K by several improvements in material production, fabrication method, preparation techniques, and so on. This number corresponds to 1800Gauss with surface peak magnetic field: Hp. It exceeds the lower critical field H_{C1} in ultrapure niobium with RRR > 2000, which is 1730Oe around 2K [1]. In addition, this achievement looks to be saturated around the 40MV/m within +3/-1MV/m in this one decade as seen in Fig.1. The variation is in the cavity shape, i.e. the differences the ratio of Hp/Eacc.

The other interesting situation was reported from Cornell University in 1997 [2]. It is on the RF critical fields of Nb, Nb_3Sn, and Pb cavities fabricated recently. Their results are shown in Fig.2. At lower temperatures with Nb cavity, the temperature dependence of RF critical field looks different from the expected one from proposed superheating field by J.Matricon and D. Saint-James [3]. Especially the theory does not fit the data in the Nb_3Sn cavity over the whole temperature rage.

The purpose of this paper is to find out a physical mechanism behind these two situations. The author reanalyzed the RF critical field of niobium cavity in detail from the superheating field considering its real temperature dependence at lower temperatures. He will conclude the vortex line nucleation as the fundamental field limitation of the RF field, which was already reported for Sn cavity by T.Yogi et al. in 1977 [4]. In this paper, the author will apply Yogi's concept to the Nb_3Sn and Pb cavities in Cornell Univ. to see the universality of the fundamental limitation mechanism in RF application, and will find a good agreement between the theory and experimental results. Finally, he will conclude the fundamental field limitation is the vortex line nucleation with both kinds of superconductors: type-I and type-II.

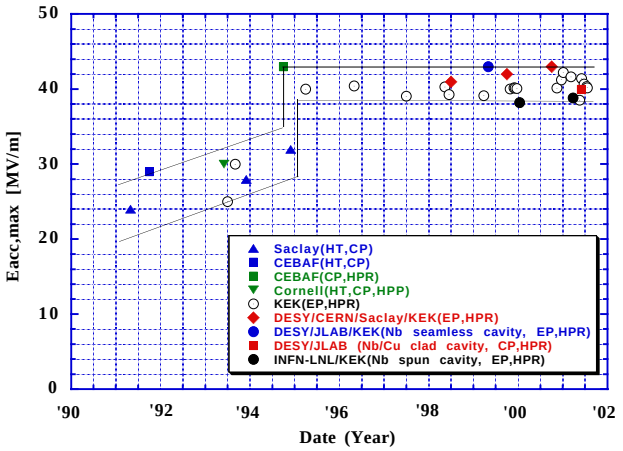

Figure 1: Saturation of the high gradient in niobium SRF cavities.

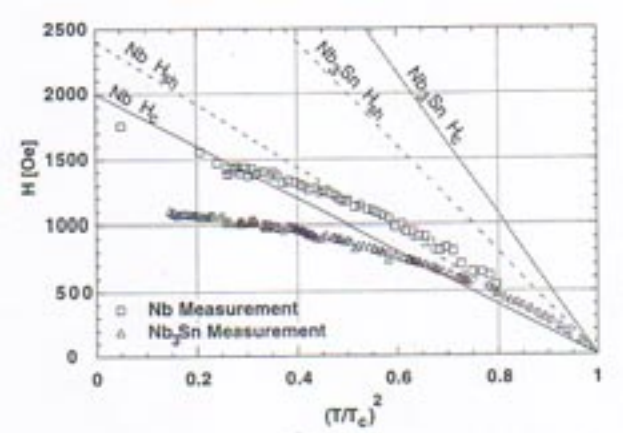

Figure 2: RF critical fields by pulse measurement in Cornell University, copied from the reference [2].

ksaito@post.kek.jp

Consideration with The Critical Field in RF Application

Niobium is a typical type II superconductor, in which the superconductor is in the Meissner state below the transition temperature T_C. Applying magnetic fields on a niobium specimen, it favours energetically flux penetrations at the lower critical field H_{C1} and leads to the mixed state, and finally goes to the normal state at the upper critical field H_{C2}. The thermo-dynamical critical field H_C is defined as:

$$F_n(T) - F_s(T) = -\int_0^{\infty} M \cdot dH = \frac{H_c^2}{8\pi} \qquad (1),$$

here F_n and F_s are the free energy per unit volume in the normal and superconducting states at a temperature T, respectively. The values of these three critical fields are in order of $H_{C1} < H_C < H_{C2}$. Therefore, in a first sight one might consider that when the maximum magnetic RF field on the cavity surface exceeds the H_{C1}, it will have a quench and be limited the gradient. This consideration however might not be right in SRF cavities. The transition at the H_{C1} is the first order and needs to a latent heat for the entropy change between two phases. It is brought by the flux penetration energy (flux nucleation) in case of type II superconductors, which relates to the surface energy in the domain wall between superconducting and normal states. The RF field amplitude varies with a time period of 10^{-8} - 10^{-9} second, which is enough short if compare with the flux nucleation time $\approx 10^{-6}$ second. So it might be possible that there should be in a meta-stable before going to the H_{C1} transition. Thus the maximum field in SRF should be higher than the H_{C1} in the type-II superconductors [5].

Belief review of RF Critical Field Experiments

Superheating is most likely the candidate for such a surface barrier against H_C with type I, or H_{C1} with type II Yogi et al. have investigated the SRF critical field in 1970's with In, Sn, Pb and their alloys Sn-In and In-Bi exposing small specimens (not cavity) in RF fields [4]. They found that the superheating rather well explains the SRF critical field qualitatively.

In 1960's, the pioneer R&D of SRF cavities has been started in Stanford University using Pb electroplated cavities or bulk niobium cavities, and the activity enlarged to other laboratories. In 1970's, niobium material became to be used more widely in SRF cavity fabrication. Currently the author believes niobium is the best material for SRF cavities. G.Meuller gave a nice review in 1986 about the high gradient in SRF cavities correcting more recent results with niobium cavities [6]. In his paper, the superheating is considered in more detail as the fundamental limitation with SRF cavities. Especially the temperature dependence is considered.

The superheating field was derived as a solution for a meta-stable sate of Ginzbrug-Landau (GL) equations in Abrikosov's theory [7], which is the theory for type II superconductors. For a deep understanding of the superheating, one has to learn about the GL Abrikosov's theory and type II superconductors, and understandings of the surface energy and the field penetration are very crucial.

This theory is very complicated and useable only for the temperature near T_C because of the perturbation theory with the order parameter or gap energy. Before going to discussion of superheating, the author would like to introduce this theory in order to have easy understanding for new comers in this SRF field.

ABRIKOSOV'S THEORY

Type II Superconductivity

That famous BCS theory was established in 1957 [8], which explains microscopically superconductivity. In those days however, many elements or a large number of alloys showed the unexpected superconducting behaviours: irreversible imperfect superconductivity (so called mixed state today), second-order transition at a higher field (so called the upper critical field H_{C2}), which was much different from the classical superconductivity (Type I superconductor). In 1957, the same year as BCS, Abrikosov published a great important paper [7], which predicts the existence of a new type (so called type II superconductor today) of reversible magnetic behaviour in superconductors obeying the Gibzburg-Landau (GL) equations [9] and having a GL parameter κ exceeding the critical value $1/\sqrt{2}$. He showed that the exact breakpoint of two kinds superconductor was at $\kappa = 1/\sqrt{2}$ considering the surface energy. Four materials with $\kappa > 1/\sqrt{2}$, he found that instead of discontinuous breakdown of classical superconductivity in a first-order transition at H_C, there was a continuous increase in flux penetration starting at a first critical field H_{C1}. And it reaches normal conducting sate at a second critical field H_{C2}, where is the second-order transition. One however believed that bulk specimens of any superconductors would, if prepared with sufficient care, exhibit the reversible, so-called ideal magnetic behaviour in the magnetization measurement like the classical superconductors. Abrikosov's theory was curiously neglected for several years until about 1962 the almost perfectly reversible behaviour was established in many pure transition elements like Ta, V, Re, Nb, and in other alloys like Pb-Tl, In-Bi, Nb_3Sn and V_3Ga etc.. These superconductors show a new thermodynamic behaviour different from the early established one as type I superconductors and his theory thus has been received for type-II superconductors.

Ginzburg Landau Equations *[10]*

Abrikosov has established his theory finding the solution of GL equations. GL theory [9], which was already proposed 7 years before BCS theory, supposes the free

energy density of superconducting state in a magnetic field (H) may be expanded in the form:

$$f_{sH} = f_{n0} + \alpha|\Psi|^2 + \frac{1}{2}\beta|\Psi|^4 + \frac{1}{2m^*}\left|(\frac{\hbar}{i}\nabla - \frac{e^*}{c}A)\Psi\right|^2 + \frac{h^2}{8\pi} \qquad (2),$$

where Ψ(r) is the order parameter and means the local density of superconducting electrons, f_{n0} is the free energy density of normal sate in zero field; e* is the effective charge; h(r) is the microscopic magnetic field; and α, β and m* are phenomenological constants. By variations of Eq.(2), one obtains the GL equations:

$$\frac{1}{2m*}\left(\frac{\hbar}{i}\nabla - \frac{e*}{c}A\right)^2\Psi + \alpha\Psi + \beta|\Psi|^2\Psi = 0 \qquad (3),$$

$$j_s = \frac{c}{4\pi}\nabla \mathrm{x}\, h = \frac{e*\hbar}{2m*i}[\Psi*\nabla\Psi - \Psi\nabla\Psi*] - \frac{(e*)^2}{m*c}|\Psi|^2 A \qquad (4).$$

In the equilibrium state, α and β are simply related to the equilibrium value of the order parameter Ψ_∞ in zero magnetic fields. They also are related to the thermo-dynamic critical field H_C:

$$|\Psi_\infty|^2 = -\frac{\alpha}{\beta} = \frac{|\alpha|}{|\beta|} \qquad (5),$$

$$f_{n0} - f_{s0} = \frac{H_c^2}{8\pi} = \frac{\alpha^2}{2\beta} \qquad (6).$$

GL equations become more simply when introduced the two characteristic parameters: penetration length λ and coherence length ξ. These parameters are given by:

$$\lambda = \sqrt{\frac{m*c^2}{4\pi N_s^*(e*)^2}} \qquad (7),$$

$$\xi = \sqrt{\frac{\hbar^2}{2m*|\alpha|}} \qquad (8),$$

where the superconducting electron density N_s^* is equal $|\Psi_\infty|^2$. It should be noticed that Eq. (7) is the same as the London penetration. In addition the Ginzbrug Landau parameter κ:

$$\kappa \equiv \frac{\lambda}{\xi} = \frac{m*}{\hbar e*}\sqrt{\frac{\beta}{2\pi}} = \frac{\sqrt{2}e*}{\hbar c}H_c\lambda^2 \qquad (9)$$

is essential to describe Abrikosov's theory. λ describes the spatial variation in the electromagnetic effect and ξ provides the spatial variations in the order parameter.

The dimensionless GL equations are convenient to calculate the superheating field later. Using the reduced $f = \Psi/\Psi_\infty$ and measuring all lengths in units as:

$$\mathbf{r}' = \frac{\boldsymbol{r}}{\boldsymbol{\lambda}},$$

$$\mathbf{h}' = \frac{\boldsymbol{h}}{\sqrt{2}}\boldsymbol{H_c},$$

$$\mathbf{A}' = \frac{\boldsymbol{A}}{\sqrt{2}}\boldsymbol{H_c\lambda},$$

$$\boldsymbol{f} = \frac{\boldsymbol{\Psi}}{|\boldsymbol{\Psi}|_\infty}$$

One can rewrite the GL Eqs.(2)-(4) to as following:

$$f_{sH} = f_{s0} + \frac{1}{4\pi}H_c^2\left\{\frac{1}{2} - f^2 + \frac{1}{2}f^4 + \left|\left[\frac{1}{i\kappa}\nabla' - A'\right]f\right|^2 + h'^2\right\} \qquad (10).$$

The dimensionless GL equations are found as:

$$\left[\frac{1}{i\kappa}\nabla' - A'\right]^2 f = f(1 - f^2) \qquad (11),$$

$$\nabla' \mathrm{x} h' = \frac{1}{2}\left\{f*\left[\frac{1}{i\kappa}\nabla' - A'\right]f + f\left[-\frac{1}{i\kappa}\nabla' - A'\right]f*\right\} \qquad (12).$$

Surface Energy

Let's see a semi-finite superconductor, of which surface is normal to $z = -\infty$ at z=0. The surface energy: σ_{ns} is defined as the difference between the actual Gibbs free energy per unit area and the value that would have if the asymptotic behavior $g_s = g_n$ at $z = \pm\infty$ held throughout the sample:

$$\sigma_{ns} \equiv \int_{-\infty}^{\infty} dz\{g_{sH} - g_n\} \qquad (13).$$

Abrikosov calculated the surface energy putting Eq.(2) into the integral of Eq.(12):

$$\sigma_{\mathrm{ns}} = \int_{-\infty}^{\infty}\left\{f_{sH} - \frac{1}{4\pi}hH_c - f_{s0}\right\}dz$$

$$= \frac{H_c^2}{8\pi}\int_{-\infty}^{\infty}\left[\left(1 - \frac{h}{H_c}\right)^2 - \left(\frac{\Psi}{\Psi_\infty}\right)^4\right]dz \qquad (14),$$

or in the dimensionless notation

$$= \frac{1}{4\boldsymbol{\pi}}\boldsymbol{H_c^2\lambda}\int_{-\infty}^{\infty}\left\{\left[\boldsymbol{h}' - \frac{1}{\sqrt{2}}\right]^2 - \frac{1}{2}\boldsymbol{f}^4\right\}\boldsymbol{dz}' \qquad (15).$$

From Eqs.(14) - (15), one notices that the surface energy can be positive or negative due to the balance of the flux expulsion energy (the first term in Eqs.(14)-(15))and the negative condensation energy (the second term in Eqs.(14)-(15).).

$\kappa(=\lambda/\xi)$ is a very important parameter to classify the superconductor. Fig.3 shows a schematic diagram of a surface layer separating normal ($z = -\infty$) and superconducting ($z = \infty$) in the material. Let's consider the configuration in Fig.3 - a). As shown in Fig.3 - a), when $\kappa \ll 1$, then $\lambda \ll \xi$ and the magnetic fields penetrate only a short distance λ into the superconductor. While the order parameter increases to its asymptotic value Ψ_∞ at a

much larger length ξ. In the region $\lambda \le z \le \xi$, the magnetic field vanishes, and the positive energy of the flux expulsion makes its full contribution. The order parameter is still appreciably small and the negative condensation energy is reduced in this region. The net surface energy is a positive in this configuration.

On the other hand, when $\kappa \gg 1$, then $\lambda \gg \xi$, the opposite situation happens. As presented in Fig.3 b), in this configuration the magnetic field penetrates a larger distance λ into the superconducting region and resulted in reduction of the positive energy of the flux expulsion for $\xi \le z \le \lambda$. In contrast, Ψ rises rapidly to its asymptotic value Ψ_∞, and the condensation energy makes its full negative contribution in the region $\xi \le z \le \lambda$. Thus the surface energy is negative. The superconductor is called type-I if σ_{ns} is positive and type-II if σ_{ns} is negative. GL Eqs. (3) and (4) cannot be integrated in closed form, even

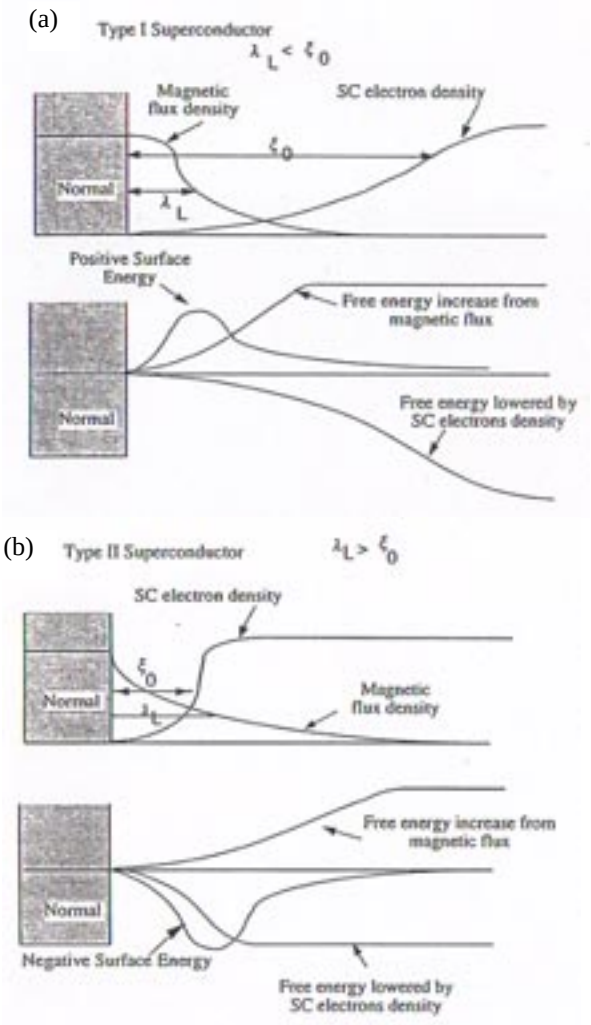

Figure 3: Schematic diagram of variation of h and f in a domain wall. (a) is for type I superconductivity and (b) for type- II, copied from [11].

for a one-dimensional configuration. Therefore, generally σ_{ns} must be calculated numerically. However, in limiting cases; $\kappa \ll 1$ and $\kappa \gg 1$ one has the following exact results:

$$\sigma_{ns} = 1.89 \cdot \xi \cdot \frac{H_c^2}{8\pi} \qquad \kappa \ll 1$$

$$\sigma_{ns} = -1.104 \cdot \lambda \cdot \frac{H_c^2}{8\pi} \qquad \kappa \gg 1$$

The critical κ value separating these two classes is at $\kappa = \frac{1}{\sqrt{2}}$, which corresponds to $\boldsymbol{\sigma_{ns} = 0}$. In Eq.(15) if

$$\sqrt{2}h' = 1 - f^2 \qquad (16),$$

$\sigma_{ns} = 0$ is guaranteed. The further calculating of a first integral of Eq.(14) or (15) shows that Eq.(16) consists with $\kappa = 1/\sqrt{2}$. The precise criterion for classification of a superconductor thus is now given as;

$$\kappa < \frac{1}{\sqrt{2}} : \text{type-I} \quad (\sigma_{ns} > 0)$$
$$\kappa > \frac{1}{\sqrt{2}} : \text{type-II} \quad (\sigma_{ns} < 0)$$

SUPERHEATING FIELD NEAR THE CRITICAL TEMPERATURE

Calculation of The Superheating Field

Superheating field: Hsh is defined as the maximum permissible value of the applied field, which satisfied GL equations. P.G.de Gennes calculated the one-dimensional Ginzburg Landau Eqs. (11) and (12) for a semi-infinite superconductor [12]. Let the field H is applied parallel to the sample, which is true for the SRF cavities, and the field directed 0-x and the vector potential along 0-y. Then the equations are:

$$\frac{1}{\kappa^2}\frac{d^2 f}{dz^2} - fA^2 + f(1 - f^2) = 0 \qquad (17)$$

$$\frac{d^2 A}{dz'^2} = f^2 A \qquad (18),$$

$$h = -\frac{dA}{dz} \qquad (19),$$

here the suffix is dropped in Eqs.(11) and (12). In the dimensionless unit, it is $H_c = 1/\sqrt{2}$. If in the Meissner state the field is expected to vanish inside of the superconductor. Here, the boundary conditions are:

$$\boldsymbol{h = H} \text{ and } \frac{\boldsymbol{df}}{\boldsymbol{dz}} = 0 \text{ at } \boldsymbol{z} = 0$$
$$\boldsymbol{A = h} = 0 \quad \text{and} \quad \boldsymbol{f} = 1 \quad \text{at } \boldsymbol{z} = +\infty$$

f should not exceed 1 and is positive. Considering the case k≫1, from Eq.(17)

$$f^2 = 1 - A^2,$$

then Eq.(18) is

$$\frac{d^2A}{dz^2} = A - A^3.$$

If multiply dA/dz on both sides, one has the following equations:

$$\frac{d}{dz}\left[\frac{1}{2}\left(\frac{dA}{dz}\right)^2 + U(A)\right] = 0$$

$$U(A) = -\frac{A^2}{2} + \frac{A^4}{4}$$

When putting the integral constant C, then one has

$$\frac{1}{2}\left(\frac{dA}{dz}\right)^2 + U(A) = C$$

For the semi-infinite superconductor as mentioned above, if imposed C=0, one obtains the solution as:

$$A(z) = \frac{\sqrt{2}}{\cosh(l - z)}$$

where l is related to the applied field H by the condition:

$$H \equiv \left(\frac{dA}{dz}\right)_{z=0} = \frac{-\sqrt{2}\sinh(l)}{\cosh^2(l)}$$

The penetration depth is in the dimensionless units:

$$\lambda = \left(\frac{A}{H}\right)_{z=0} = [-\tanh(l)]^{-1}$$

When $\sinh(l) = -1$, the maximum permissible H is obtained:

$$\boldsymbol{H_{sh} = \frac{1}{\sqrt{2}}, \quad = H_c} \textbf{ in the dimentionless units}$$

For $\kappa \to \infty$, the superheating field should be the thermo-dynamical field H_C. For the low-κ limit, the GL approximation gives the superheating field as [13]:

$$H_{sh} = \frac{H_c}{(\sqrt{2}\cdot\kappa)^{1/2}}$$

For other κ, the superheating field cannot be calculated by analytic method and has to be performed a numerical integration of Eqs. (17)-(19). Matricon and Saint-James made the calculation [3]. Their result is presented in Fig.4. When one fits the result as a function of κ in the region $\kappa > 1/\sqrt{2}$, he gets the following formula:

$$\boldsymbol{H_{sh} = \frac{1.291}{\kappa^{0.160}}\cdot H_c}$$

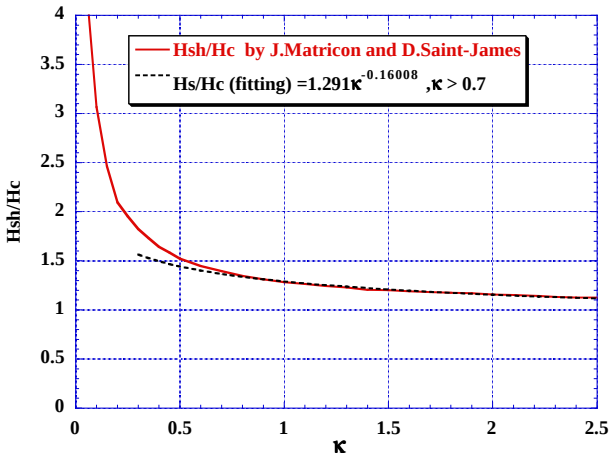

Figure 4: Superheating field calculated by J.Matricon and D. Saint-James [3].

Physical Intuitional Consideration for H_{sh}

Plane Nucleation

Above the calculation on superheating field is complicate. It is difficult to have physical image. Here, let's see more intuitional consideration about it. The superheating might be related to the surface energy. By a rough discussion, a linear approximation might be possible with λ and ξ in Fig.3. The diagram then becomes a triangle configuration. In this simple configuration, the surface energy may be

$$\sigma_{ns} = \frac{1}{8\pi}\lambda H^2 - \frac{1}{8\pi}\xi H_c^2 \qquad (20)$$

here, the super-condensation energy (negative) per unit volume is considered as $-H_c^2/8\pi$ at $z = \infty$. Supposing when one apply fields on a superconductor, it makes the transition to normal conducting state at $\sigma_{ns} = 0$, the permitted applied field is:

$$\frac{1}{8\pi}\lambda H^2 - \frac{1}{8\pi}\xi H_c^2 \geq 0 \quad \text{for type I}$$

$$\frac{1}{8\pi}\lambda H^2 - \frac{1}{8\pi}\xi H_c^2 \leq 0 \quad \text{for type II}$$

This simple consideration gives the superheating field for type I superconductors:

$$H_{sh} = \sqrt{\frac{\xi}{\lambda}}H_c = \frac{1}{\sqrt{\kappa}}H_c \quad \text{for type I} \qquad (21).$$

In this superheating, flux nucleation should be happened in the plane penetrated fields. Therefore it is called plane nucleation. In contrast, for Type II, Eq.(21) gives the smaller field than H_C. If κ is larger enough, it will be smaller than H_{C1}. Thus the simple consideration is not available for Type-II of the superheating.

Vortex Line Nucleation

Another intuitional nucleation is a line nucleation of a vortex. In this case as seen in Fig.5, the condensation energy (f_{core}) is canceled by the energy brought by the applied field (f_{mag}). Thus the following energy balance is realized:

$$\frac{1}{8\pi}(\lambda H)^2 = \frac{1}{8\pi}(\xi H_c)^2 \;\Rightarrow\; \lambda H = \xi H_c$$

Then superheating field is:

$$H_{sh} = \frac{\xi}{\lambda} H_c = \frac{1}{\kappa} H_c \qquad (22).$$

This superheating is called as vortex line nucleation and is valid for both superconductors.

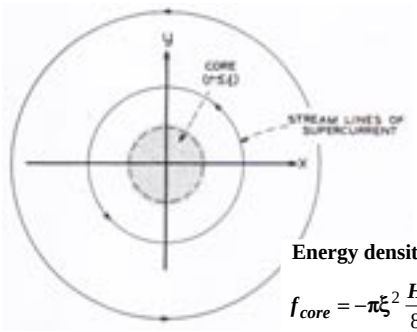

Energy density per unit vortex line

$$f_{core} = -\pi\xi^2 \frac{H_c^2}{8\pi}, \quad f_{mag} = \pi\lambda^2 \frac{H_c^2}{8\pi}$$

Figure 5: Vortex line nucleation.

Summary of Superheating

Here, the predictions of superheating are summarized in Table 1.

Table 1: Predictions of superheating

Prediction	Hsh	Availability
J.P. Burger and D.Saint-Jamis	H_c	$\kappa >> 1$
J.Matricon and D.Saint-James*	$\frac{1.291\mathbf{H_c}}{\boldsymbol{\kappa}^{0.160}}$	$\kappa \geq \frac{1}{\sqrt{2}}$
Vortex Line Nucleation	$\frac{H_c}{\kappa}$	all κ
Plane Nucleation	$\frac{H_c}{\sqrt{\kappa}}$	$\kappa \leq \frac{1}{\sqrt{2}}$
Orsay Group	$\frac{H_c}{\sqrt{2^{1/2}\kappa}}$	$\kappa << 1$

*The fitted result in this work to make clear the κ dependence.

MESURMENT OF MAGNETIC CHARACTERRISTICS

Now we have finished preparation for data analysis of the critical field with niobium cavities. When one considers the temperature dependence in the formulas in Table1, he can compare the results with experimental ones. Focused thing in this paper is to find the formula of Hsh temperature dependent with niobium. This is done using the formulas in Table 1 by using the temperature dependences of H_C and κ. κ(T) will be determined by the temperature dependences of H_C, H_{C1} and H_{C2}. So the next step is to investigate the material properties of niobium. However, here before going to the subject, more instructive descriptions are given for new comers about the measurement methods such magnetic properties and magnetization curve, and so on.

Measurement of magnetic flux penetration

Fig.6 [14] shows a very simple measurement for flux penetration. Fig.7 is the real measurement set-up in KEK [15]. Fig.8 presents the examples of measurement results. On the specimen, a pick-up coil is wound fine wire by several hundred turns. The ends of this coil are connected to a voltage-meter. A magnetic field H is applied parallel to the axis of the specimen by a superconducting solenoid coil. When the field is increased gradually with a constant speed, by the Faraday's low an induced voltage appears on the pick-up coil as:

$$\phi = \mu_0 H(t)\cdot(S_1 + S_s),\; H(t) = H_0 t$$
$$V = -\frac{d}{dt}\phi = -\mu_0 H_0 S_g - \mu_0 H_0 \frac{d}{dt} S_s$$

where S_g is a gap area between the surface of the specimen and pick-up coil if there is and S_s an area of the cross-section of the specimen. Up to the H_{C1}, the specimen is in the Meissner state and field cannot enter the inside of the specimen, thus S_S=0 and only a constant induced voltage by the gap appears on the voltage-meter. When the field crosses over the H_{C1}, flux penetration starts and a step-like signal occurs on the pick-up coil at H_{C1}. Increasing the field further the specimens show

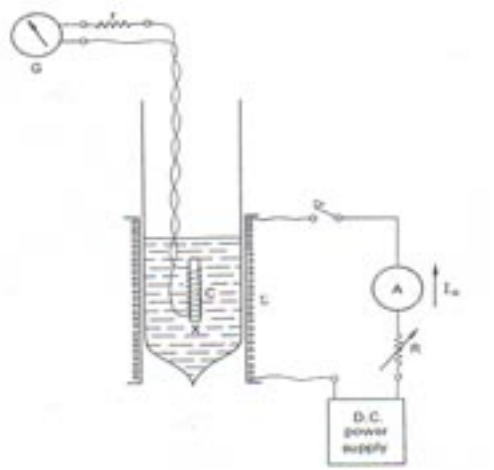

Figure 6: Magnetic penetration measurement, copied from the reference [14].

various kind of signals, for instance with a well-annealed sample, which is presented in Fig.8 (niobium material), the signal exponentially smoothly decreases after the step-like signal at H_{C1} and then reaches a constant voltage at H_{C2}, which is determined by the sample cross-section area. In the case of sample with defects, many spick-like signals appear due to the flux trapping. After chemical etching such a sample by 100μm, the spick-signals disappear and a similar signal is observed with the well anneal sample. Anyway this method is very simple but one can observe the dynamical flux penetration phenomena.

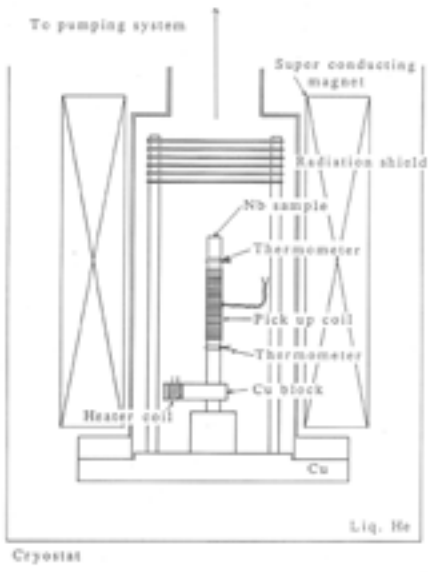

Figure 7: Magnetic flux penetration measurement apparatus in KEK.

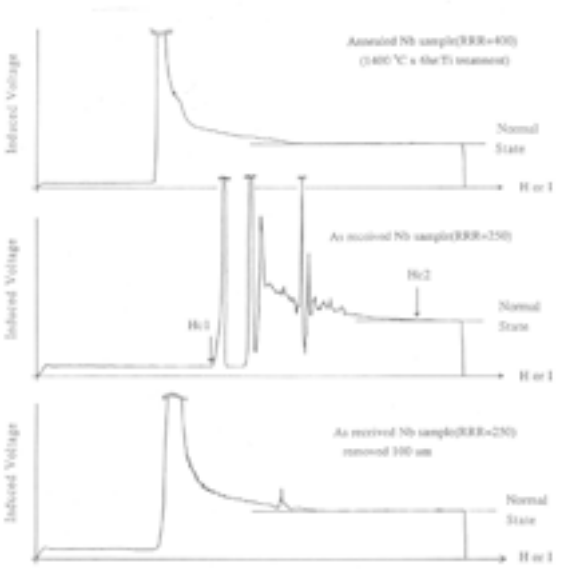

Figure 8: Examples of output signal in the pickup coil.

Measurement of Magnetization

In the formulas of superheating, H_C is as important as κ. H_C is obtained by the integration of the magnetization curve as seen Eq.(1). Fig.9 shows the magnetization curve measurement method. The specimen is wound pick-up coil. The other pick-up coil, which is identical to the first pick up coil but wound in opposite direction of the first coil on the specimen, is connected in series. When increasing the solenoid field H with a constant speed, the similar phenomenon happens as before. However, only the magnetization can be observed because the voltage induced outside of the sample can be cancelled each other as following:

$$V = V_A - V_B \propto \frac{d}{dt}\mu_0(H+M) - \frac{d}{dt}\mu_0 H$$
$$\propto -\frac{d}{dt}M$$

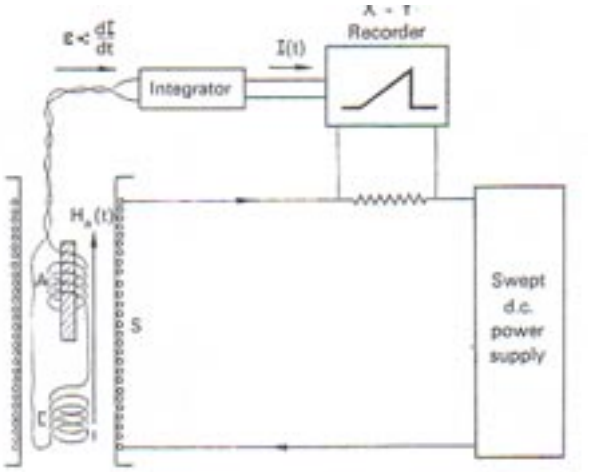

Figure 9: Principle of measurement of magnetization, copied from [14].

The output signal is put into an electronic integrator, a circuit whose output voltage is related to the input signal by $V_{out} \propto \int V_{in} dt$. The output of the integrator is therefore:

$$V_{out} \propto \int_0^t \frac{d}{dt} M dt = M .$$

USEFUL FORMULAS BY ABRIKOSOV'S THEORY

We must evaluate λ and ξ of niobium material and calculate κ. These parameters can be calculated by useful formulas with H_{C1}, H_{C2} or H_C [10]. It will be of worth to describe about those parameters to understand the formulas.

H_{C1}

From a thermo-dynamical consideration, H_{C1} is determined as

$$H_{c1} = \frac{4\pi n\varepsilon_1}{B} = \frac{4\pi n\varepsilon_1}{n\phi_0} \quad (23),$$

where ε_1 is one flux nucleation energy per unit volume, B induction field, n flux line density and

$$\phi_0 = hc/2e = 2.07\text{x}10^{-7}\, Gauss/cm^2$$

is the fluxoid quantum. Eq.(23) assumes the noninteraction flux lines. ε_1 is calculated by both the London equation and Abrikosov's solution of the GL equations. Hc1 is then given for $\lambda/\xi >> 1$:

$$H_{c1} = \frac{\phi_o}{4\pi\lambda^2}\ln(\frac{\lambda}{\xi}) \quad \text{by L-theory} \quad (24)$$

$$H_{c1} = \frac{\phi_o}{4\pi\lambda^2}\ln(\frac{\lambda}{\xi} + 0.08) \quad \text{by A-theory} \quad (25)$$

Both theories lead the very close results.

The relationship with H_C is given as:

$$\frac{H_{c1}}{H_c} = \frac{\ln(\kappa + 0.08)}{\sqrt{2}\kappa} \quad (26).$$

On the other hand, the relation ship with H_{C2} is:

$$\frac{H_{c1}}{H_{c2}} = \frac{\ln(\kappa + 0.08)}{2\kappa^2} \quad (27).$$

The temperature variations of H_{C1} ,H_C and H_{C2} are given in Fig.10 with ultra-pure niobium with RRR>2000. The empirical temperature variation of H_{C1} is:

$$\boldsymbol{H_{c1}(T)} = 1850.0 \cdot [1 - \left(\frac{\boldsymbol{T}}{\boldsymbol{T_c}}\right)^2] \quad (28),$$

and is very close to that of H_C. A linear relationship with H_{C1} and H_C is presented in Fig.11, is fitted for every temperature below T_C as:

$$H_{c1}(T) = 0.9469 \cdot H_c(T) \quad (29).$$

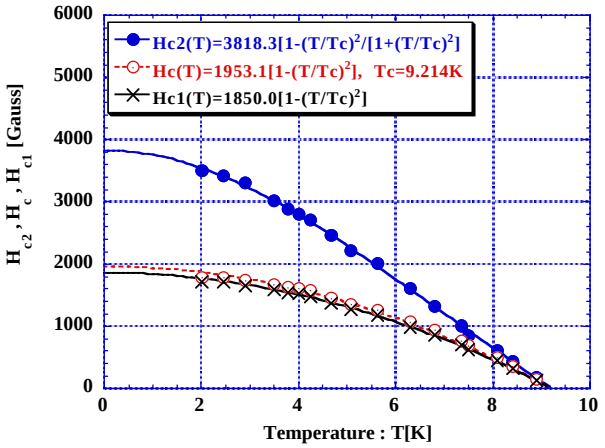

Figure 10: Temperature dependences of H_{C1}, Hc and H_{C2} of ultrapure niobium with RRR>2000 (Data by A.French in the reference [1]).

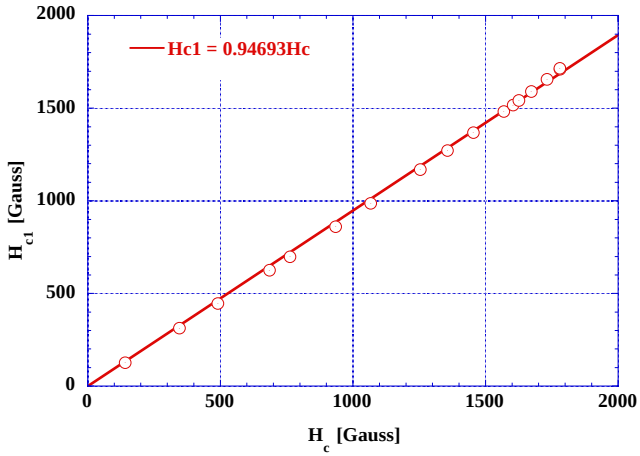

Figure 11: The linear relationship between Hc1 and H_C in the ultra-pure niobium.

H_C

H_C is very important to evaluate λ. Eq.(9) is rewritten using the quantum fluxoid as:

$$H_c = \frac{\kappa}{\lambda^2}\frac{\hbar c}{\sqrt{2}e^*} = \frac{\kappa}{\lambda^2}\frac{(hc/2e)}{2\pi\sqrt{2}} = \frac{\phi_0}{2\pi\sqrt{2}\lambda\xi} \quad (30),$$

where e*=2e is used. This is another important formula. When one knows ξ, λ is directly calculated from Eq.(30).

For both type superconductors, the temperature variation of H_C is found as:

$$H_c(T) = H_c(0)\left[1 - \left(\frac{T}{T_c}\right)^2\right] \quad (31).$$

BCS model calculation shows the agreement with Eq.(31) within 4% in all temperature range below T_C. In Fig.9 for ultrapure niobium, the temperature variation is given as:

$$H_c(T) = 1953.1 \cdot [1 - \left(\frac{T}{T_c}\right)^2] \quad (32),$$

and is well fitted with T_C=9.214K.

H_{C2}

When the applied field H is increased up to H_{C2}, type II superconductors have a new thermodynamic transition, which is of second order. In near the transition, f is small enough so that GL Eqs (11) and (12) may be linearized. We thus have following dimensionless equations

$$\left[\frac{1}{i\kappa}\nabla - A\right]^2 f - f = 0 \quad (33)$$

$$A = H\vec{e}_y x \quad (34)$$

here, the semi-infinite sample surface is normal to $x = -\infty$. This linearized equation then become:

$$\left[-\frac{1}{\kappa^2}\nabla^2 + i\frac{2H}{\kappa}x\left(\frac{\partial}{\partial y}\right) + H^2\right] f = f \quad (35)$$

The general solution is of the form:

$$f = \exp(ik_y y + ik_z z)u(x),$$

where u(x) satisfies the one-dimensional harmonic oscillator equation:

$$u'' + \left[\kappa^2 - k_z^2 - (H\kappa x - k_y)^2\right]u = 0 \qquad (36).$$

The eigenvalue is gives as:

$$\frac{(\kappa^2 - k_z^2)}{H\kappa} = 2n + 1$$

The discrete eigenvalue thus is:

$$H^{(n)} = \frac{\kappa^2 - k_z^2}{\kappa(2n+1)} \qquad (37).$$

H_{C2} is expected the highest possible critical field, and it occurs n=0 and kz=0. Thus an important formula concerning to H_{C2} is obtained:

$$H_{c2} = \kappa \quad \text{in dimensionless unit}$$
$$H_{c2} = \sqrt{2}\kappa H_c \quad \text{in conventional unit} \qquad (38).$$

This is a most important formula to obtain the κ-value. If one knows both temperature variations of H_{C2} and H_C, that of κ is directly calculated by Eq.(38) . This can be rewritten more useful expression for calculation of ξ, if inputting Eq.(30) into Eq.(38):

$$H_{c2} = \sqrt{2}\frac{\lambda}{\xi}\frac{\phi_0}{2\pi\sqrt{2}\lambda\xi} = \frac{\phi_0}{2\pi\xi^2} \qquad (39).$$

This is another important formula to calculate ξ and its temperature dependence. As shown later, from the temperature variation of ξ(T), the expected temperature variation is given as:

$$\boldsymbol{H_{c2}(T) = \frac{\phi_o}{2\pi\xi^2(0)}\cdot\frac{1-(T/T_c)^2}{1+(T/T_c)^2}} \qquad (40)^*.$$
$$= \boldsymbol{H_{c2}(0)\cdot\frac{1-(T/T_c)^2}{1+(T/T_c)^2}}$$

As seen in Fig.9, for the pure niobium with RRR>2000 it is given as:

$$H_{c2}(T) = 4111.5\cdot\frac{1-(T/T_c)^2}{1+(T/T_c)^2},\ T_c = 9.301K \qquad (41)$$

Temperature Dependence of λ

This is well established. The theoretical formula of the temperature dependence of London penetration-depth λ_L was given by Daunt in 1947 [16], who suggested combining the London's original expression for λ with the Gorter-Casimir two-fluid equation [17], where n_s is replaced by the temperature dependent number of super-electrons: $n_s(t) = n_s(0)(1-t^4)$ and therefore it is given:

$$\lambda_L(t) = \frac{\lambda_L(0)}{\sqrt{1-t^4}} \qquad (42),$$

where $\lambda_L(0) = \sqrt{mc^2/\left[4\pi e^2 n_s(0)\right]}$ and t is the reduced temperature: T/T_C. This temperature variation, which is called today empirical formula, well agrees with experiment results when $\xi_0 << \lambda_L(T)$(London limit). Here ξ_0 is defined as:

$$\xi_0 = 0.18\frac{\hbar v_F}{k_B T_c}$$

Small deviations from the form (42) have been observed at very low reduced temperatures, and these can be explained by BCS theory.

The experimental value of λ can be calculated from the experimental $H_C(T)$ and $H_{C2}(T)$ using Eqs.(30) and (39) as:

$$\frac{H_{c2}(T)}{H_c(T)} = \sqrt{2}\cdot\frac{\lambda(T)}{\xi(T)} \qquad (43),$$

$$\xi(T) = \sqrt{\frac{\phi_o}{2\pi\cdot H_{c2}(T)}} \qquad (44).$$

As seen in Eq.(39), the temperature variation of ξ is directly obtained from $H_{C2}(T)$ experimental result. Then one can put the result into Eq.(43), thus one has the experimental temperature dependence of λ. Such a calculation result with pure niobium is presented in Fig12. Eq.(42) fits the experimental result very nicely with λ(0)=419.22Å and T_C=9.2143K as fitting parameters. In the ultrapure niobium case, the fitting result is:

$$\lambda(T) = \frac{419.22}{\sqrt{1-(T/T_c)^4}},\ T_c = 9.2143K \qquad (45),$$

where the unit is in Angstrom.

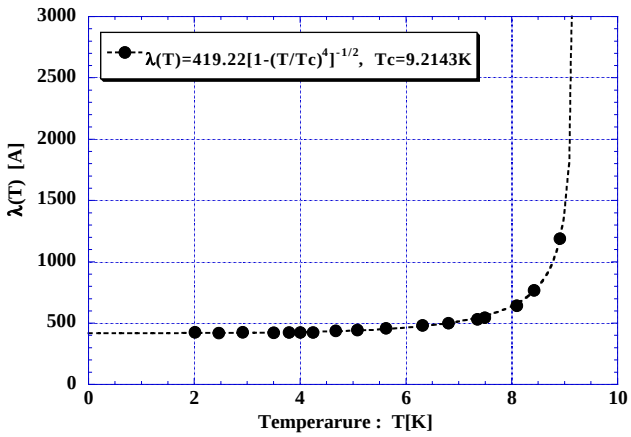

Figure 12: Fitting result by Eq.(42) of the temperature variation of λ. Calculated using French's data [1].

*The author finally reached this formula, which can lead the correct ξ(T) as seen later. However, today it is known as the Abrikosov-Ginzburg formula. He did not know it by near finishing this paper.

Temperature Variation of ξ

The temperature variation ξ(T) is directly calculated by Eq.(44) from the experimental $H_{C2}(T)$. The results should be fitted the following formula:

$$\xi(T)=\frac{\phi_o}{2\pi\sqrt{2}\lambda(T)\cdot Hc(T)}=\frac{\phi_o}{2\pi\sqrt{2}\lambda(0)\cdot Hc(0)}\cdot\sqrt{\frac{1+(T/T_c)^2}{1-(T/T_c)^2}} \qquad (46).$$
$$=\xi(0)\sqrt{\frac{1+(T/T_c)^2}{1-(T/T_c)^2}}$$

In GL theory the other formula is often used at a temperature near the transition temperature T_C [18]:

$$\xi(T)=\frac{\xi(0)}{\sqrt{1-(T/T_c)}} \qquad (47)^*.$$

However, Eq.(47) produces the linier function with T for $H_{C2}(T)$ as seen in Fig.13 The experimental $H_{C2}(T)$ usually has a saturation at lower temperature. It cannot represent the saturation. We thus use Eq.(46) as the temperature variation of ξ in this paper. Fig14 shows ξ(T) with the ultrapure niobium by the experimental $H_{C2}(T)$. Both formulas fit the experimental result very nicely with the same fitting goodness:

$$\xi(T)=282.63\sqrt{\frac{1+(T/T_c)^2}{1-(T/T_c)^2}},\ T_c=9.3023K \qquad (48),$$
$$\text{or}\quad =\frac{260.08}{\sqrt{1-(T/T_c)}},\ T_c=9.2299K$$

where the unit is in Angstrom.

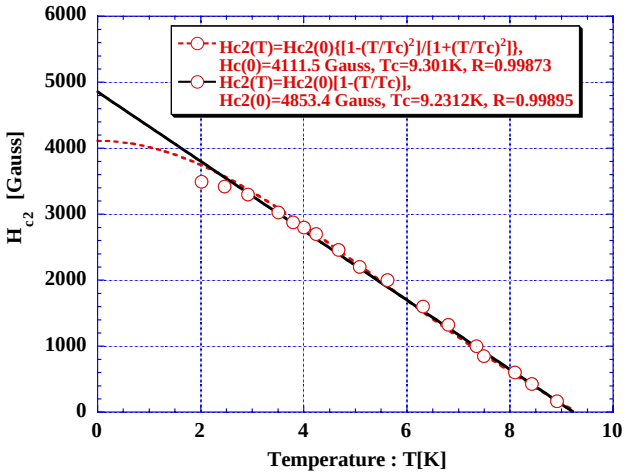

Figure 13: Comparison of the temperature dependence with H_{C2} between Eqs.(46) and (47).

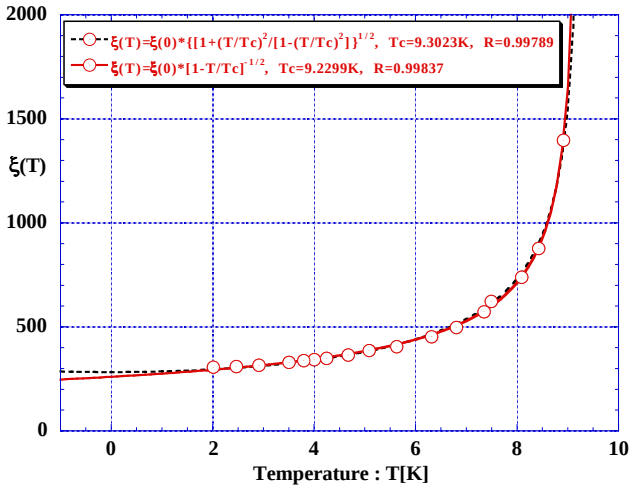

Figure 14: Comparison of fitting the temperature variation of ξ between Eqs.(46) and (47).

Temperature Dependence of κ

κ(T) is also directly calculated from the experimental $H_{C2}(T)$ and $H_C(T)$. The result is presented in Fig.14 for the ultrpure niobium. The data should be fitted by the following formula:

$$\kappa(T)\equiv\frac{\lambda(T)}{\xi(T)}=\frac{H_{c2}(T)}{\sqrt{2}H_c(T)}=\frac{H_{c2}(0)}{\sqrt{2}\cdot H_c(0)}\cdot\frac{1}{1+\left(\frac{T}{T_c}\right)^2} \qquad (49).$$
$$=\frac{\kappa(0)}{1+\left(\frac{T}{T_c}\right)^2}$$

For the ultra-pure niobium, the fitting result is as:

$$\kappa(T)=\frac{1.508}{1+\left(\frac{T}{T_c}\right)^2} \qquad (50).$$

With niobium, one will find that κ-value is larger

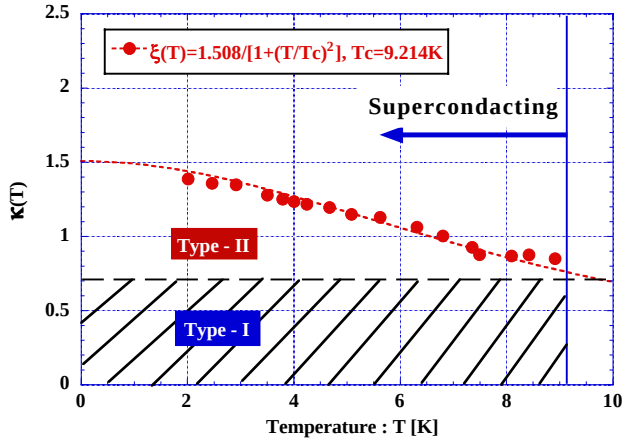

Figure 15: Temperature variation of κ with ultrapure Niobium [1] and the fitting by Eq.(50).

* If one uses this formula, he will lead a wrong temperature dependence of the superheating field.

than $1/\sqrt{2}$ in every temperature blow Tc, thus niobium is a well-defined type II superconductor. In addition, one has to notice that the value increases with decreasing temperature.

MAGNETIC PROPERTIES OF THE INDUSTRIALLY PRODUCED NIOBIUM MATERIAL

The above measured magnetic properties of niobium are for well annealed and ultra-pure material in a lab level. In SRF cavity production, industrially produced niobium material is used. To date such niobium material has the RRR=200~300 in standard. We need to know the magnetic property with such a material, which might be different behavior from the ultra-pure specimen. We measure the H_{C1} and H_{C2} for the niobium specimens from Tokyo Denkai by the method in Fig.6. The niobium sample has RRR=246 as received and RRR=398 after annealing at 1400°C with titanium.

RRR=246 Nb Material

This sample was cut from niobium sheet with RRR=246 and chemically polished by 100microns using 1:1:1 (nitric acid/hydrofluoric acid/phosphoric acid). The size is 5mm wide, 2.5 mm thick and 150mm long. The cross section is a square but the corners are rounded a little bit. A pick up coil with 250 tunes was wound on the sample. An example of signal is seen in the bottom of Fig.8. Fig.16 is the result of temperature variation measurement with H_{C1} and H_{C2}. H_C was calculated presuming the same relationship in Eq.(29). T_C was 8.8K and a little bit low comparing with ultrapure material: Tc=9.25K. Data fitting gives the following results:

$$H_{c1}(T) = 1948.6[1-(T/T_c)^2],\ T_c = 8.827K \quad (51),$$

$$H_c(T) = 2057.8\cdot[1-(T/T_c)^2] \quad (52),$$

$$H_{c2}(T) = 4921.0\cdot\frac{[1-(T/T_c)^2]}{[1+(T/T_c)^2]} \quad (53).$$

Fig.17 shows ξ(T) by Eq.(44), λ(T) by Eqs.(44) and (43). By the best fitting following results are given:

$$\xi(T) = 262.27\sqrt{\frac{1+(T/T_c)^2}{1-(T/T_c)^2}},\ T_c = 8.9456K \quad (54),$$

$$\lambda(T) = \frac{433.6}{\sqrt{1-(T/T_c)^4}},\ T_c = 8.718K \quad (55),$$

where the unit is in Angstrom.

Fig.18 is the temperature variation of κ calculated by Eq.(49). Best fitting gives the results with a similar fitting accuracy:

$$\kappa(T) = \frac{1.6109}{1+(T/T_c)^2},\ T_c = 10.037K \quad (56).$$

where the unit is in Angstrom. Best fitting result gives a little bit higher Tc=10.0K.

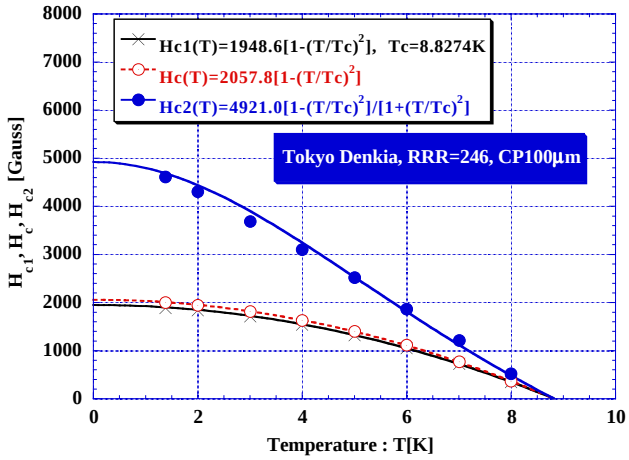

Figure 16: Temperature variations of H_{C1}, H_C and H_{C2} with RRR=246 Nb material from Tokyo Denkai.

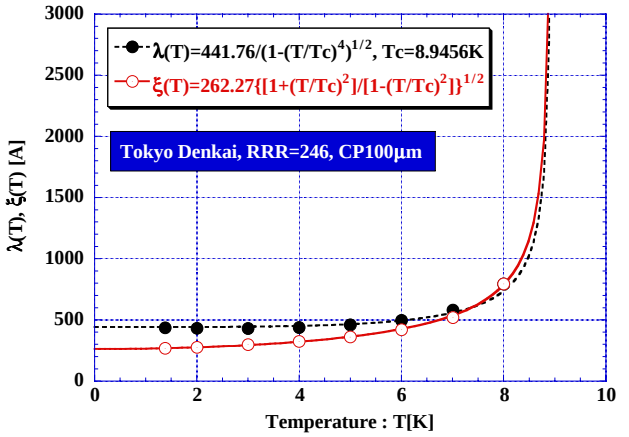

Figure 17: Temperature variations of ξ and λ with RRR=246 Nb material from Tokyo Denkai.

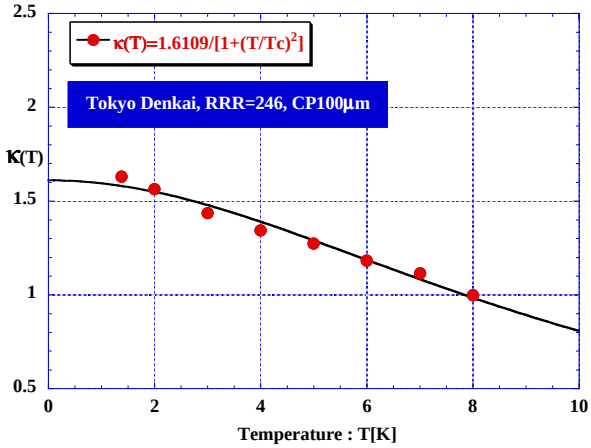

Figure 18: Temperature variation of κ with RRR=246 Nb material from Tokyo Denkai.

1400°C Annealed Material

The sample was cut from the RRR=246 niobium sheet from Tokyo Denkai and annealed at 1400°C for 3 hours with titanium getter. The resultant RRR was 398. Fig.18 is the $H_{C1}(T)$ and $H_{C2}(T)$ and $H_C(T)$. Best fitting gives the following results:

$$H_{c1}(T) = 1908.5[1-(T/T_c)^2],\quad T_c = 9.0138K \qquad (57),$$

$$H_c(T) = 2015.6\cdot[1-(T/T_c)^2],\quad T_c = 9.0138K \qquad (58)$$

$$H_{c2}(T) = 4565.1\cdot\frac{[1-(T/T_c)^2]}{[1+(T/T_c)^2]},\quad T_c = 9.0419K \qquad (59).$$

Fig.20 shows the ξ(T) and λ(T). Best fitting gives the following results:

$$\xi(T) = 266.0\sqrt{\frac{1+(T/T_c)^2}{1-(T/T_c)^2}},\quad T_c = 8.9687K \qquad (60),$$

$$\lambda(T) = \frac{428.03}{\sqrt{1-(T/T_c)^4}},\quad T_c = 8.9267K \qquad (61).$$

Fig.21 is the best fitting result with the κ(T). Best fitting gives the results with a similar fitting accuracy:

$$\kappa(T) = \frac{1.6005}{1+(T/T_c)^2},\quad T_c = 9.1952K \qquad (62)$$

As seen in comparison with Fig.18 and Fig.21, such a high temperature annealing effects on the κ-value close to T_C, which makes the value smaller. However the κ-vale at the low temperatures T < 3K changes little by the high temperature annealing.

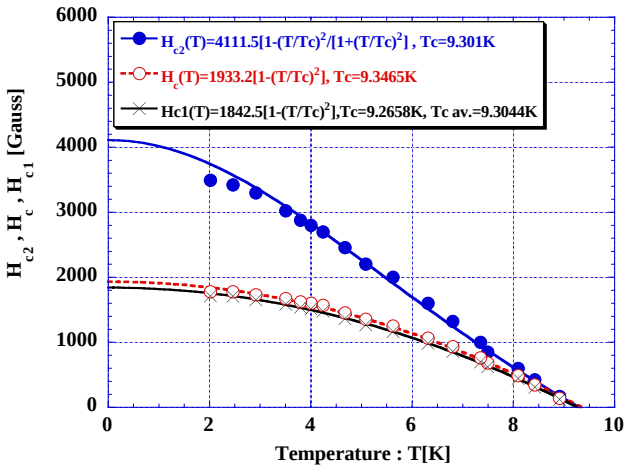

Figure 19: Temperature variations of H_{C1}, H_C, and H_{C2} with 1400°C annealed (RRR=398) Nb material.

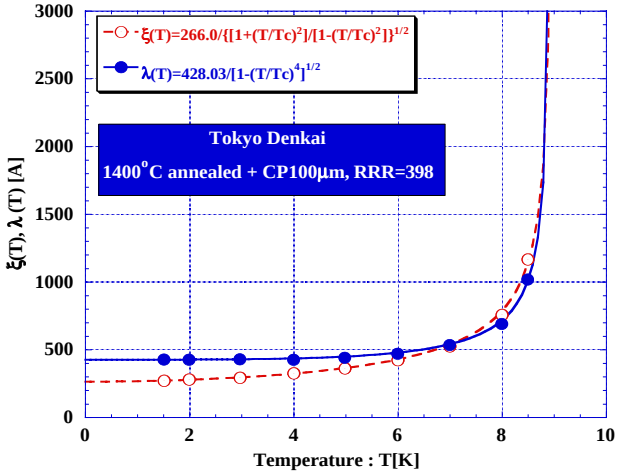

Figure 20: Temperature variations of ξ and λ with 1400°C annealed (RRR=398) Nb material.

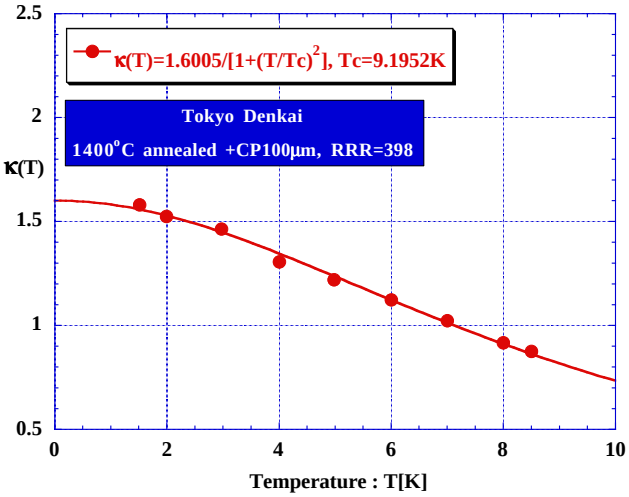

Figure 21: Temperature variation of κ with 1400°C.

Summaries of Material Parameters

The best fitted magnetic parameters are summarized in Table 2 to 7. Fig. 22 shows the RRR dependence of normalized material parameters by those of the ultrapure niobium.

Table 2: Fitting results with H_{C1} (T) for various RRR.

RRR	$H_{c1}(T) = H_{c1}(0)\cdot\left[1-\left(\frac{T}{T_c}\right)^2\right]$	
	$H_{c1}(0)$ [Gauss]	T_C [K]
246	1948.6	8.827
398	1908.5	9.014
> 2000	1850.0	9.214

Table 3: Fitting results with H (T) for various RRR.

RRR	$H_c(T) = H_c(0)\cdot\left[1-\left(\frac{T}{T_c}\right)^2\right]$	
	$H_c(0)$ [Gauss]	T_c [K]
246	2057.8	8.827
398	2015.6	9.014
> 2000	1953.1	9.214

Table 4: Fitting results with H_{C2} (T) for various RRR

RRR	$H_{c2}(T) = H_{c2}(0)\cdot\frac{1-(T/T_c)^2}{1+(T/T_c)^2}$	
	$H_{c2}(0)$ [Gauss]	T_c [K]
246	4921.0	8.827
398	4565.1	9.012
> 2000	4111.5	9.301

Table 5: Fitting results with λ(T) for various RRR

RRR	$\lambda(T) = \frac{\lambda(0)}{\sqrt{1-(T/T_c)^4}}$	
	$\lambda(0)$ [Å]	T_c [K]
246	433.6	8.718
398	428.0	8.927
> 2000	419.2	9.214

Table 6: Fitting results with ξ(T) for various RRR

RRR	$\xi(T) = \xi(0)\cdot\sqrt{\frac{1+(T/T_c)^2}{1-(T/T_c)^2}}$	
	$\xi(0)$ [Å]	T_c [K]
246	262.3	8.946
398	266.0	8.969
> 2000	282.6	9.302

Table 7: Fitting results with κ(T) for various RRR

RRR	$\kappa(T) = \frac{\kappa(0)}{1+(T/T_c)^2}$	
	$\kappa(0)$ [Å]	T_c [K]
246	1.611	10.037
398	1.601	9.195
> 2000	1.508	9.214

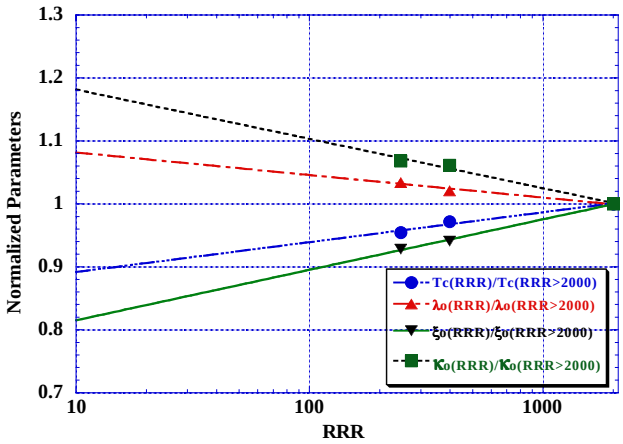

Figure 22: The RRR dependence of T_C, λ, ξ, and κ, which are normalized those of ultra-pure niobium material with RRR~2000.

COMPARISONS OF RF CRITICAL FIELD BETWEEN THEORY AND EXPERIMENTS

In the comparison with theories and the experimental critical fields, one thing should be reminded. The results in Table 1 are superheating fields for DC field. The superheating is basically fixed by energy balance in the flux nucleation. Therefore, when one compares DC superheating fields with RF filed measurement, he must use the effective strength for the RF field, i.e.

$$H \to \frac{1}{\sqrt{2}}H$$

This requires to multiple the factor $\sqrt{2}$ to the DC superheating field in the Table 1. Here, the temperature dependent formulas for Maticon and Saint-James (MSM) model, the vortex line nucleation model (VLNM) and the plane nucleation model are given as:

$$H_{sh}(T) = \sqrt{2}\cdot 1.291\cdot\frac{H_c(T)}{\kappa^{0.160}(T)} = 1.826\cdot\frac{H_c(0)}{k^{0.160}(0)}\cdot\left[1-(T/T_c)^2\right]\cdot\left[1+(T/T_c)^2\right]^{0.160}$$

for MSM (63),

$$H_{sh}(T) = \sqrt{2}\cdot\frac{H_c(T)}{k(T)} = \sqrt{2}\cdot\frac{H_c(0)}{k(0)}\cdot\left[1-(T/T_c)^4\right]$$

for VLNM (64),

$$H_{sh}(T) = \sqrt{2}\cdot\frac{H_c(T)}{\sqrt{\kappa(T)}} = \sqrt{2}\cdot\frac{H_c(0)}{\sqrt{\kappa(0)}}\cdot[1-(T/T_c)^2]\cdot[1+(T/T_c)^2]^{\frac{1}{2}}$$

for Plane Nucleation. (65).

Nb Cavity Case

Here the author compares $H_{sh}(T)$ between the above theories and experiments. In Fig.22, black circles are Cornell results by pulse measurements with a 1300 MHz cavity produced by Russian high-RRR material and post-purified by solid-state gettering to 1000 RRR. Crossing marks are KEK results with 1300MHz niobium bulk cavities with RRR=200 - 400. As seen before, the

annealing effects on κ(T) at the temperature close to T_C and the effect is less at the lower temperature T <3K. Here, using the fitting parameters for the 1400°C annealed niobium material in this work, the Hsh(T) for MSM, VLNM and Plane nucleation with niobium are given as:

$$H_{sh}(T) = 1.826\frac{2015.6}{1.601^{0.160}}\cdot\left[1-(T/9.014)^2\right]\cdot\left[1+(T/9.014)^2\right]^{0.160}$$
$$= 3413.5\cdot\left[1-(T/9.014)^2\right]\cdot\left[1+(T/9.014)^2\right]^{0.160}$$
for MSM (66),

$$H_{sh}(T) = \sqrt{2}\cdot\frac{2015.6}{1.601}\cdot\left[1-(T/9.014)^4\right]$$
$$= 1780.4\cdot\left[1-(T/9.014)^4\right]$$
for VLNM (67).

$$H_{sh}(T) = \sqrt{2}\cdot\frac{2015.6}{\sqrt{1.601}}\cdot[1+(T/9.014)^2]^{\frac{1}{2}}\cdot[1-(T/9.014)^2]$$
$$= 2252.8\cdot[1+(T/9.014)^2]^{\frac{1}{2}}\cdot[1-(T/9.014)^2]$$
for Plane Nucleation (68).

The Cornell data [2] was fitted by these formulas (66) – (68) in Fig. 22. VLNM can fit the experimental results rather satisfactorily with both the absolute value and the temperature dependence, while MSM and Plane nucleation cannot fit both. The author did not know the detail Yogi's works by obtaining his doctoral thesis. In 1976, he already pointed the temperature dependence of the critical field in it as [3]:

$$\frac{H_{sh}}{H_c}\Big|_{plane} \propto [1+(T/T_c)^2]^{\frac{1}{2}}$$ for plane nucleation (69),

$$\frac{H_{sh}}{H_c}\Big|_{line} \propto [1+(T/T_c)^2]$$ for line nucleation (70),

$$\frac{H_{sh}}{H_c}\Big|_{point} \propto [1+(T/T_c)^2]^{\frac{3}{2}}$$ for point nucleation (71),

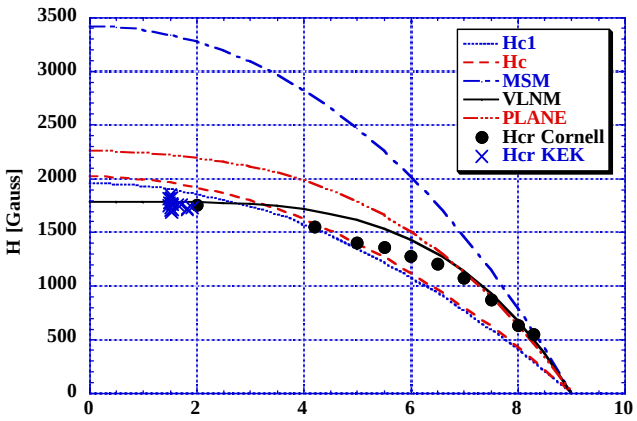

Figure 23: Comparison of Hsh(T) between the theories and experiments.

of which first two formulas are same as in this work. He has pointed that the pure samples with tin and indium (both are type I superconductors) have a vortex-like nucleation as the critical field. In case of pure niobium also, the RF critical magnetic field is more likely the vortex line nucleation.

Nb_3Sn Cavity Case

It is very curious to see how the VLNM fits the result of Nb_3Sn [2], which is a typical type- II superconductor. In this case, $H_c(0)/\kappa(0)$ and T_C were fitted as free parameters in Eq.(64). Fig.24 shows the fitting results by the three kinds of model: plane nucleation, vortex line nucleation and point nucleation, which correspond to the formula (69) to (71), respectively. Only the VNLM model can fit the result over the temperature range. The fitting result of VLNM is gives as:

$$H_{sh}(T) = 1033.3\cdot[1-(T/18.226)^4]$$ (72).

When one uses the fitting result:

$$1033.3 = \sqrt{2}\cdot\frac{H_c(0)}{\kappa(0)},$$

if used $H_C(0)$=5400 Gauss [5], the κ(0) is calculated as 7.39, which is the reasonable result.

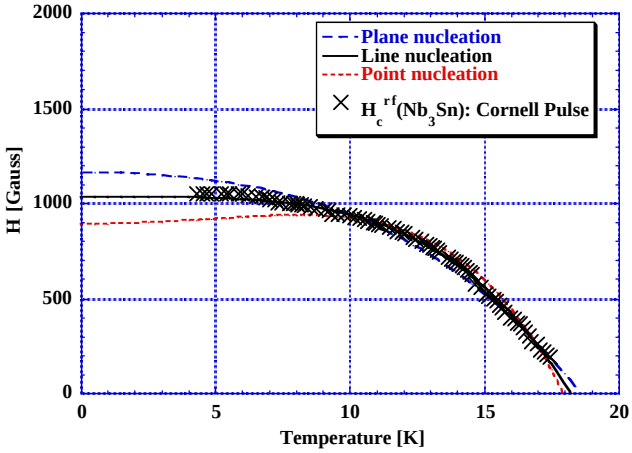

Figure 24: Fitting results of the experimental RF critical field with Nb_3Sn cavity in Cornell Uni [2].

Pb Cavity Case

As pointed by Yogi, in case of type I the RF critical field more likely is limited by vortex line nucleation. Pb is a type I superconductor. As shown in Fig.25, Cornell has measure the RF critical field of a Pb cavity [2]. Let's fit their results. In this case also the result was fitted by the three models. The resultant fitted formulas are:

$$H_{sh}(T) = 720.23\cdot[1-(T/7.322)^4]$$ for VLNM (73),

$$H_{sh}(T) = 795.86 \cdot [1 + (T / 7.643)^2]^{\frac{1}{2}} \cdot [1 - (T / 7.643)^2]$$
for Plane Nucleation (74),

$$H_{sh}(T) = 632.92 \cdot [1 + (T / 7.105)^2]^{\frac{3}{2}} \cdot [1 - (T / 7.105)^2]$$
for Point Nucleation (75).

VLNM gives a quite good fitting result and is consistent with Yogi's statement. Plane nucleation also shows the good fitting. Table 8 shows the fitted parameters for the case three cases. In our analysis, κ(0) and $H_C(0)$ are not fitted independently. $H_C(0)$ was fixed as 804 Gauss [5] when κ(0) is calculated in Table 8. Every fitting result shows a rather large κ(0) value, which corresponds to type II superconductor. Our results are for electroplated lead material and it might be different from the pure lead. Anyway we need to measure such material properties by the method mentioned in the section 4.

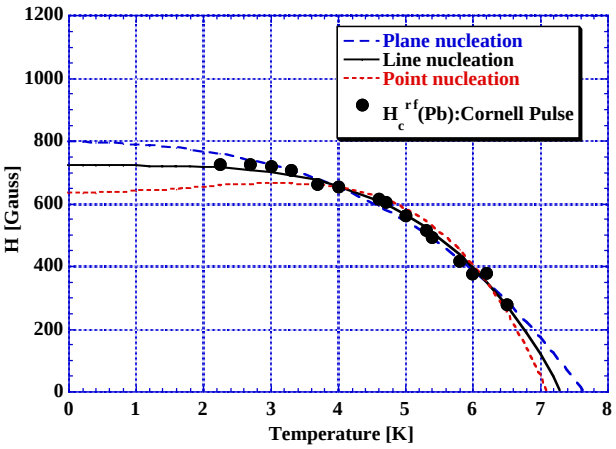

Figure 25: Fitting results of the experimental RF critical field with Pb cavity in Cornell Uni. [2].

Table 8: Fitted parameter by the three cases for Pb cavity.

Models / Parameters	Line	Plane	Point	Other experiment [18]
T_C [K]	7.32	7.64	7.11	7.2
$H_C(0)$ [Gauss]	(804)	(804)	(804)	804
κ(0)	1.58	2.04	1,48	0.5

CONCLUSION

So far the author has presented the long description about superconductor to find Hsh(T). For the vortex line nucleation, the superheating field is calculated as:

$$H_{sh} = \sqrt{2} \cdot \frac{H_c}{\kappa}.$$

The temperature dependence of Hc is well known as:

$$H_c(T) = H_o \cdot \left[1 - (T / T_c)^2\right].$$

Therefore, finding the Hsh(T) is reduced to find κ(T). On the other hand, since κ is calculated as:

$$\kappa \equiv \frac{1}{\sqrt{2}} \cdot \frac{H_{c2}}{H_c},$$

one has Hsh(T) automatically, when $H_{C2}(T)$ is obtained. The author made a lot of effort and finally reached the formula of $H_{C2}(T)$:

$$H_{c2}(T) = H_{c2}(0) \cdot \frac{1 - \left(\frac{T}{T_c}\right)^2}{1 + \left(\frac{T}{T_c}\right)^2}.$$

This is already well known as the Abrikosov-Ginzburg formula, but he did not noticed until his near finishing the paper. He finally obtained the Hsh(T) as:

$$H_{sh}(T) = \sqrt{2} \cdot \frac{H_c(0)}{\kappa(0)} \cdot \left[1 - (T / T_c)^4\right].$$

When the superheating field was calculated using this formula, it developed that the formula can fit nicely the experimental critical field with Nb, Nb_3Sn and Pb cavities. This result strongly suggests the theoretical critical field of superconducting RF cavities is vortex line nucleation. This is the first conclusion in this paper.

The second conclusion is that niobium cavity, of which material is expected as the best material for sc cavities, has already reached the fundamental field limitation by the current cavity production technology. Thus, the saturation of the high gradient around 40MV/m is explained as due to the theoretical field limitation of niobium material.

As seen in Fig.26, the RRR dependence of Hsh(T=0) from the material investigation of niobium is very small,

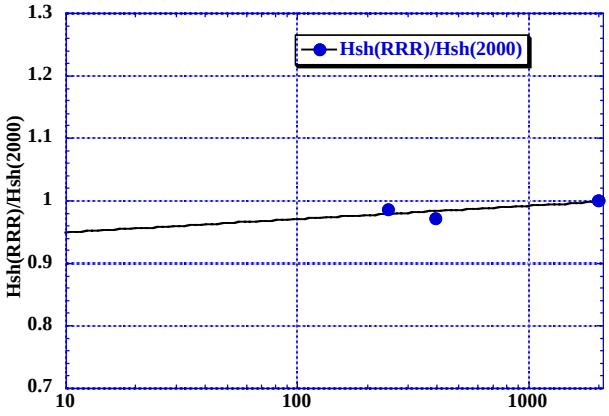

Figure 26: RRR dependence of the superheating field with niobium.

i.e. 5% increase even at RRR~2000, therefore any great improvement in the high gradient cannot be expected in

high RRR niobium materials. Since the Hsh(0) is ~1800 Gauss, if one hopes Eacc = 50 MV/m, which will be needed for the TESLA-1000, he has to make new cavity design with a small ratio of Hp/Eacc, for example Hp/Eacc=36 Gauss/(MV/m). This is the third conclusion. Fortunately, we have already such a cavity design by J Sekutowicz et al. in JLAB [19]. To choose a smaller iris diameter is an easy way to reduce the ratio but the smaller cell-to-cell coupling becomes other problem with trapping modes. Thus the number of cell should be reduced in the extremely high gradient cavity structure. The superstructure of 7-cell might be a most attractive for the TESLA-1000.

The final conclusion is that on the high gradient there is no hope in the cavities by high T_C material like Nb_3Sn, if this analysis is right.

REFERENCES

[1] R. A French, "Intrisic Type-2 Superconductivity in Pure Niobium", Cryogenics 8, 1968, pp.301- 308.

[2] T. Hays and H. Padamsee, "Measuring the RF Critical Field of Pb, Nb, and Nb_3Sn", Proc. of the 8th Workshop on RF Superconductivity, Padova, Italy, Oct. 6 – 10, 1997, pp.789 – 794.

[3] J.Matricon and D.Saint-James, "Superheating Field in Superconductors", Phys. Lett. Vol. 24A, No.8, 1967. pp.241-242.

[4] T.Yogi, in his doctoral thesis, "Radio Frequency Studies of Surface Resistance and Critical Magnetic Field of Type I and Type II Superconductors", California Institute of Technology, Pasadena, California, USA, 1997.

[5] H.Piel, "Superconducting Cavities", CERN Accelerator School (1988) pp.149-196.

[6] G. Meuller, "Superconducting Niobium in High RF Magnetic Fields", Proc. of the 3rd Workshop on RF Superconductivity, Argonne, Illinois, USA, Sept.14 – 18, 1987, pp.331 – 358.

[7] A.A.Abrikosov, "On the Magnetic Properties of Superconductors of the Second Group", Soviet Phys. JETP, Vo.5. No.6, 1957. pp. 1174 – 1182.

[8] J.Bardeen, L.N. Cooper, and J.R. Schrieffer, Phys. Rev. 108, 1957, pp. 1175.

[9] V.L. Ginzburg and L.D. Landau, Zh. Eksperim. I Teor. Fiz. 20, 1950, pp. 1064.

[10] in this paper, referred the following textbooks," Introduction to Superconductivity", by M.Tinkham, McGRAW-HILL BOOK COMPANY, New York, 1973
and "Superconductivity" I and II edited by R.D. Parks, MARCE DEKKER, INC., New York, 1969.

[11] the textbook by H.Padamsee et al., "RF Superconductivity for Accelerators", Jhon Wiley & Sons, INC. 1998. pp.99 – 102.

[12] P.G. de Gennes, "Vortex Nucleation in Type II Superconductors", Solid State Com. Vol.31965, pp.127 – 130.

[13]V. L. Ginzburg, Zh. Eksp. Teor. Fiz. 34, 113 (1958), Sov. Phys. JETP 7, 78(1958)

[14] Textbook, "Introduction to Superconductivity" by A.C. Rose-Innes and E.H. Rhoderik, Pergamon Press in 1969.

[15] K.Saito et al., "TESLA Activities at KEK", Proc. of the 6th Workshop on RF Superconductivity, Newport News, Virginia, USA, Oct. 4 – 8, 1993, pp.372 – 381.

[16] J.G. Daunt, Phys. Rev. 72,89(1947).

[17] C.J.Gorter and H.B.G.Casimir, Phyik, Z. 35, 963 (1934); Z.Tech. Phys. 15,539 (1934).]

[18] for example, in the textbook "Introduction to Superconductivity", by M.Tinkham, McGRAW-HILL BOOK COMPANY, New York, 1973, pp.112 – 113.

[19] J Sekutowicz et al., " Cavities for JLAB's 12GeV Upgrade", Proc. of the PAC2003, in Portland, USA, pp. 1395 – 1397.